ISSN 1392-2114 ULTRAGARSAS, Nr.1(42). 2002.

Plotting moire fringes for high frequency vibrations of shell type structures from FEM results

M. Ragulskis[1], L.Ragulskis[2+]

[1]*Kaunas University of Technology*

[2]*University Vytautas Magnum*

Introduction

Procedures for plotting computer generated moire mechanical interference bands (moire fringes) from the results of finite element analysis can provide meaningful information about the processes taking place in the analysed structures. Such visualisation is important from the point of view of interpretation of experimental results [2], [8] and enables calculation of structural stresses with sufficient accuracy [1], [9]. Computer generated moire fringes produced from the overlap of two repetitive patterns can give realistic view of the structural deformations. Moreover, the digital plotting procedures of moire fringes can be also effectively applied for the visualisation of periodic dynamic processes if the structure is stroboscopically photographed in the states of equilibrium and the states of extreme displacements.

Numerical generation of realistic fringe patterns requires non-trivial computer code implementations. The sufficient smoothness of the interfering grids must be considered. That requires the utilisation of multiple intensity levels and incorporation of 3D graphical models. On the other side, the discrete FEM results must be interpolated over the domain of the structure. Visualisation of small deformations around the state of equilibrium without exaggerating the nodal displacements also requires appropriate adaptations.

The commonly used repetitive patterns for the generation of moire fringes are interference grids formed from arrays of parallel straight lines. Application of such grids for the three dimensional shell type structures faces quite severe complications due to the variable thickness of the lines.

Therefore the numerical procedures generating realistic moire fringe patterns for different structural geometries are important and useful tools for visualisation of numerical analysis data and interpretation of experimental results.

Construction of moire fringe patterns for two dimensional problems

It is assumed that FEM analysis is based on the linear theory of elasticity. Therefore, if the nodal deformations (or amplitudes of harmonic oscillation used for stroboscopic analysis) in the direction of the x and y axes are defined as u and v it is possible to find the original locations of points in the state of equilibrium, when their positions in the deformed structure are defined. If the coordinates of a point on the deformed surface are (α, β), then this point in the state of equilibrium has the coordinates $(\alpha - u, \beta - v)$. This reconstruction may be performed for any interpolated point on the analysed surface. Such a methodology enables the preservation of the optical shape of the structure and eliminates the need for exaggerating small deformations around the status of equilibrium.

In order to obtain better interpretable moire fringes the smooth variation of the intensity of the fringes on the surface of the object is proposed. It is assumed that the intensity varies according to the harmonic law. The intensities of lines on the object in the state of equilibrium correspond to the first term in the following expressions, the other term corresponds to the deformed status of the structure:

$$I = \cos^2\left(\frac{2\pi\alpha}{\lambda}\right) + \cos^2\left(\frac{2\pi(\alpha - u)}{\lambda}\right), \quad (1)$$

$$I = \cos^2\left(\frac{2\pi\beta}{\lambda}\right) + \cos^2\left(\frac{2\pi(\beta - v)}{\lambda}\right), \quad (2)$$

where λ is the constant defining the distance between the grid lines, I stands for a intensity level, (1) represents the isothethes of u, (2) represents the isothethes of v.

The concept of isothethes is used in the description of moire fringes in [1] and concerns the image obtained by the overlapping of the image of the lines on the structure in equilibrium and in the deformed status.

Two maps must be built separately for identifying moire fringes in appropriate directions. The direction of the parallel grid lines can be varied by elementary rotations of the structure.

It can be noted, that the interpretation of moire isothethes is not trivial. Fig. 1 shows the geometry of the structure in equilibrium (grey lines) and the third eigenmode (dark solid lines) of a rectangular plate with fastened lower edge. It is assumed that the displacements in both directions on the lower edge of the plate in the state of plain stress are equal to zero, elsewhere the structure is free.

The external excitation is not stated explicitly and is assumed to be harmonic with the resonant frequency of this eigenmode and is not orthogonal to it. Thus it is possible to excite this only mode (assuming it is not multiple) with

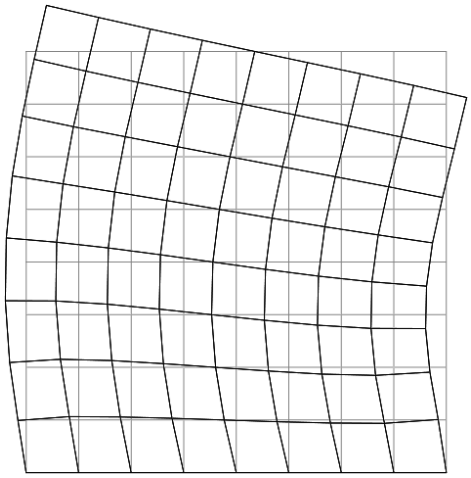

Fig. 1. **The geometry and the third eigenmode of the plate**

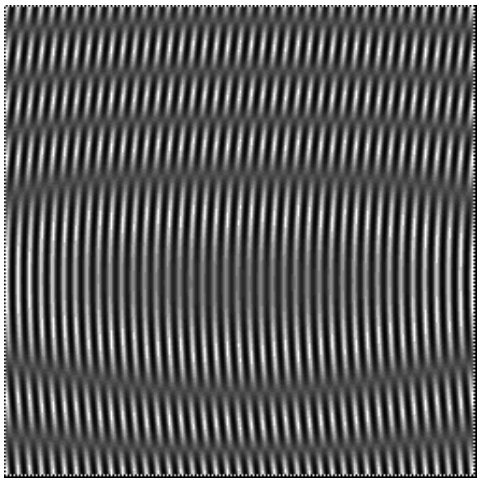

Fig. 2. **Generated moire fringes for the displacement in the direction of the *x* axis**

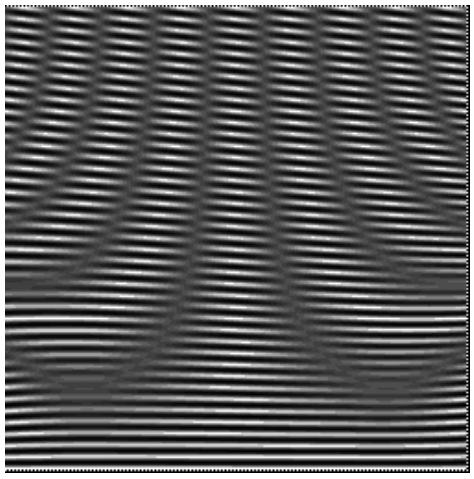

Fig. 3. **Generated moire fringes for the displacement in the direction of the *y* axis**

negligible contribution of the other modes, and to analyse its steady state motion by using stroboscopic photographing. The nodal displacements are exaggerated with respect to the dimensions of the structure, the mesh is quite coarse.

The constructed moire fringe patterns in two planar directions are presented in Fig. 2 and Fig. 3.

Isolines represent the lines on the surface of the structure on which the analysed quantity takes constant values. The density of isolines indicates the rapidity of change of the represented quantity. The presented methodology enables generation of smooth moire patterns from relatively rough FEM approximation.

Moire fringes for three dimensional shell type structures

The amplitudes of harmonic oscillations used for stroboscopic analysis in the directions of the *x, y* and *z* axes are defined as *u, v* and *w*. If the coordinates of a point on the deformed surface are (α, β, γ), then this point in the state of equilibrium has the coordinates $(\alpha - u, \beta - v, \gamma - w)$.

Isolines of displacements in both directions are constructed to validate the formation of isothethes (Fig. 4 and Fig. 5).

The intensities are calculated on the basis of (1), (2) and the following relationship:

$$I = \cos^2\left(\frac{2\pi\gamma}{\lambda}\right) + \cos^2\left(\frac{2\pi(\gamma - w)}{\lambda}\right), \tag{3}$$

where the latter equation represents the isothethes of *w*.

The element used is similar to the described in [4], but involves the transformation of rotations to the tangential direction similarly to [5]. The nodal variables are the displacements in the directions of the axes of coordinates *u, v, w* and the rotations in the tangential directions Θ_r, Θ_t. Here the subscripts indicate the tangential directions.

The derivatives of the coordinates *x, y, z* in the directions of the local axes ξ, η are:

$$\begin{bmatrix} N_{1\xi} & N_{2\xi} & \cdots \\ N_{1\eta} & N_{2\eta} & \cdots \end{bmatrix} \cdot \begin{bmatrix} x_1 & y_1 & z_1 \\ x_2 & y_2 & z_2 \\ \vdots & \vdots & \vdots \end{bmatrix} = \begin{bmatrix} x_\xi & y_\xi & z_\xi \\ x_\eta & y_\eta & z_\eta \end{bmatrix} \tag{4}$$

where x_i, y_i, z_i are the coordinates of the *i*-th node, N_i – the *i*-th shape function of the finite element; the subscripts ξ, η denote partial derivatives with respect to the local coordinates.

The matrix of the direction cosines at the point of integration is:

$$[T] = \begin{bmatrix} r_x & r_y & r_z \\ t_x & t_y & t_z \\ p_x & p_y & p_z \end{bmatrix} \tag{5}$$

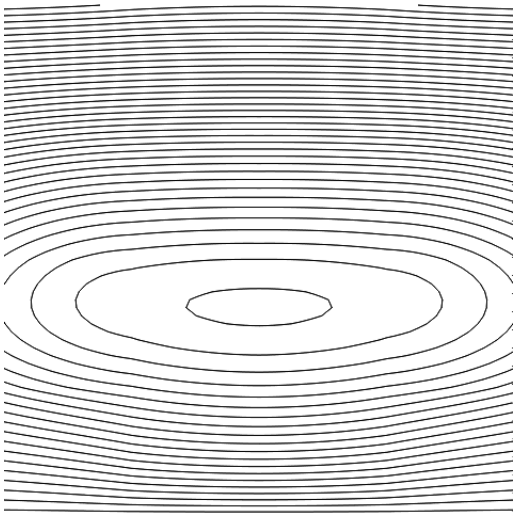

Fig. 4. **The isolines of the displacement in the direction of the *x* axis**

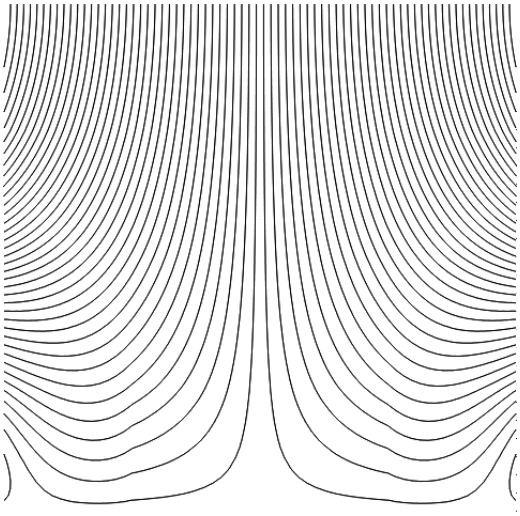

Fig. 5**. The isolines of the displacement in the direction of the *y* axis**

where:

$$\begin{Bmatrix} p_x \\ p_y \\ p_z \end{Bmatrix} = \left\| \begin{Bmatrix} x_\xi \\ y_\xi \\ z_\xi \end{Bmatrix} \times \begin{Bmatrix} x_\eta \\ y_\eta \\ z_\eta \end{Bmatrix} \right\|^{-1} \cdot \left(\begin{Bmatrix} x_\xi \\ y_\xi \\ z_\xi \end{Bmatrix} \times \begin{Bmatrix} x_\eta \\ y_\eta \\ z_\eta \end{Bmatrix} \right) = \\ = \begin{pmatrix} (y_\xi z_\eta - z_\xi y_\eta)^2 + \\ + (z_\xi x_\eta - x_\xi z_\eta)^2 + \\ + (x_\xi y_\eta - y_\xi x_\eta)^2 \end{pmatrix}^{-0,5} \cdot \begin{Bmatrix} y_\xi z_\eta - z_\xi y_\eta \\ z_\xi x_\eta - x_\xi z_\eta \\ x_\xi y_\eta - y_\xi x_\eta \end{Bmatrix} \tag{6}$$

$$\begin{Bmatrix} r_x \\ r_y \\ r_z \end{Bmatrix} = \left\| \begin{Bmatrix} x_\xi \\ y_\xi \\ z_\xi \end{Bmatrix} \right\|^{-1} \cdot \begin{Bmatrix} x_\xi \\ y_\xi \\ z_\xi \end{Bmatrix} = \\ = \frac{1}{\sqrt{x_\xi{}^2 + y_\xi{}^2 + z_\xi{}^2}} \cdot \begin{Bmatrix} x_\xi \\ y_\xi \\ z_\xi \end{Bmatrix}, \tag{7}$$

$$\begin{Bmatrix} t_x \\ t_y \\ t_z \end{Bmatrix} = \begin{Bmatrix} p_x \\ p_y \\ p_z \end{Bmatrix} \times \begin{Bmatrix} r_x \\ r_y \\ r_z \end{Bmatrix} = \begin{Bmatrix} p_y r_z - p_z r_y \\ p_z r_x - p_x r_z \\ p_x r_y - p_y r_x \end{Bmatrix}, \tag{8}$$

where $\{r\}$, $\{t\}$ and $\{p\}$ form the orthonormal base on the middle surface of the shell element. $\{r\}$ and $\{t\}$ are tangential to the surface, $\{p\}$ is normal to it.

The Jacobian of the change of the variables of differentiation is calculated as:

$$\begin{bmatrix} r_\xi & t_\xi \\ r_\eta & t_\eta \end{bmatrix} = \begin{bmatrix} x_\xi & y_\xi & z_\xi \\ x_\eta & y_\eta & z_\eta \end{bmatrix} \cdot \begin{bmatrix} r_x & t_x \\ r_y & t_y \\ r_z & t_z \end{bmatrix}. \tag{9}$$

The change of the variables of differentiation is performed on the basis of the equations:

$$\begin{bmatrix} N_{1r} & N_{2r} & \cdots \\ N_{1t} & N_{2t} & \cdots \end{bmatrix} = \begin{bmatrix} r_\xi & t_\xi \\ r_\eta & t_\eta \end{bmatrix}^{-1} \cdot \begin{bmatrix} N_{1\xi} & N_{2\xi} & \cdots \\ N_{1\eta} & N_{2\eta} & \cdots \end{bmatrix}. \tag{10}$$

The rotations about the directions of the axes of coordinates Θ_x, Θ_y, Θ_z are related with the tangential rotations as:

$$\begin{Bmatrix} \Theta_x \\ \Theta_y \\ \Theta_z \end{Bmatrix} = \begin{Bmatrix} r_x \\ r_y \\ r_z \end{Bmatrix} \Theta_r + \begin{Bmatrix} t_x \\ t_y \\ t_z \end{Bmatrix} \Theta_t . \tag{11}$$

The following matrixes are formed:

$$[N] = \begin{bmatrix} N_1 & 0 & 0 & 0 & 0 & N_2 & \vdots & \\ 0 & N_1 & 0 & 0 & 0 & 0 & \vdots & \cdots \\ 0 & 0 & N_1 & 0 & 0 & 0 & \vdots & \end{bmatrix},$$

$$[B_r] = \begin{bmatrix} N_{1r} & 0 & 0 & 0 & 0 & N_{2r} & \vdots & \\ 0 & N_{1r} & 0 & 0 & 0 & 0 & \vdots & \cdots \\ 0 & 0 & N_{1r} & 0 & 0 & 0 & \vdots & \end{bmatrix},$$

$$[B_t] = \begin{bmatrix} N_{1t} & 0 & 0 & 0 & 0 & N_{2t} & \vdots & \\ 0 & N_{1t} & 0 & 0 & 0 & 0 & \vdots & \cdots \\ 0 & 0 & N_{1t} & 0 & 0 & 0 & \vdots & \end{bmatrix}, \tag{12}$$

$$\left[\overline{N}\right]=\begin{bmatrix}0&0&0&N_1r_{x1}&N_1t_{x1}&0&\vdots&\\0&0&0&N_1r_{y1}&N_1t_{y1}&0&\vdots&\cdots\\0&0&0&N_1r_{z1}&N_1t_{z1}&0&\vdots&\end{bmatrix},$$

$$\left[\overline{B_r}\right]=\begin{bmatrix}0&0&0&N_{1r}r_{x1}&N_{1r}t_{x1}&0&\vdots&\\0&0&0&N_{1r}r_{y1}&N_{1r}t_{y1}&0&\vdots&\cdots\\0&0&0&N_{1r}r_{z1}&N_{1r}t_{z1}&0&\vdots&\end{bmatrix},$$

$$\left[\overline{B_t}\right]=\begin{bmatrix}0&0&0&N_{1t}r_{x1}&N_{1t}t_{x1}&0&\vdots&\\0&0&0&N_{1t}r_{y1}&N_{1t}t_{y1}&0&\vdots&\cdots\\0&0&0&N_{1t}r_{z1}&N_{1t}t_{z1}&0&\vdots&\end{bmatrix},$$

where $\begin{Bmatrix}r_{xi}\\r_{yi}\\r_{zi}\end{Bmatrix}$ and $\begin{Bmatrix}t_{xi}\\t_{yi}\\t_{zi}\end{Bmatrix}$ are tangential orthonormal vectors at node i.

The interpolated variables are transformed to the local directions $\{r\}$, $\{t\}$ and $\{p\}$:

$$\begin{aligned}\left[N^*\right]&=[T]\cdot[N],\\ \left[B_r{}^*\right]&=[T]\cdot[B_r],\\ \left[B_t{}^*\right]&=[T]\cdot[B_t],\\ \left[\overline{N}^*\right]&=[T]\cdot\left[\overline{N}\right],\\ \left[\overline{B_r}^*\right]&=[T]\cdot\left[\overline{B_r}\right],\\ \left[\overline{B_t}^*\right]&=[T]\cdot\left[\overline{B_t}\right].\end{aligned}\qquad(13)$$

In the following formulas the numerical subscript denotes the row number of the previous matrixes.

The stiffness matrix is calculated as:

$$[K]=\iint\left(\begin{array}{l}[B]^T[D][B]+\\+\left[\overline{B}\right]^T\left[\overline{D}\right]\left[\overline{B}\right]+\left[\overline{\overline{B}}\right]^T\left[\overline{\overline{D}}\right]\left[\overline{\overline{B}}\right]\end{array}\right)drdt\,,\qquad(14)$$

where

$$[D]=h\begin{bmatrix}\frac{E}{1-\nu^2}&\frac{E\nu}{1-\nu^2}&0\\ \frac{E\nu}{1-\nu^2}&\frac{E}{1-\nu^2}&0\\ 0&0&\frac{E}{2(1+\nu)}\end{bmatrix},$$

$$\left[\overline{D}\right]=\frac{h^2}{12}[D],\qquad(15)$$

$$\left[\overline{\overline{D}}\right]=\frac{Eh}{2(1+\nu)k}\begin{bmatrix}1&0\\0&1\end{bmatrix},$$

$$[B]=\begin{bmatrix}\left[B_r{}^*\right]_{(1)}\\ \left[B_t{}^*\right]_{(2)}\\ \left[B_t{}^*\right]_{(1)}+\left[B_r{}^*\right]_{(2)}\end{bmatrix},$$

$$\left[\overline{B}\right]=\begin{bmatrix}\left[\overline{B_r}^*\right]_{(2)}\\ -\left[\overline{B_t}^*\right]_{(1)}\\ \left[\overline{B_t}^*\right]_{(2)}-\left[\overline{B_r}^*\right]_{(1)}\end{bmatrix},\qquad(16)$$

$$\left[\overline{\overline{B}}\right]=\begin{bmatrix}\left[B_t{}^*\right]_{(3)}-\left[\overline{N}^*\right]_{(1)}\\ \left[B_r{}^*\right]_{(3)}+\left[\overline{N}^*\right]_{(2)}\end{bmatrix},$$

where E is the modulus of elasticity; ν is the Poisson's ratio; h is the thickness of the shell; k is the shear correction factor in order to account for the actual distribution of the shear stresses assumed to be equal to 1,2.

The mass matrix is calculated as:

$$[M]=\iint\left(\begin{array}{l}\left[N^*\right]^T\rho h\left[N^*\right]+\\+\left[\overline{N}^*\right]^T\frac{\rho h^3}{12}\begin{bmatrix}1&0&0\\0&1&0\\0&0&0\end{bmatrix}\left[\overline{N}^*\right]\end{array}\right)drdt\,,\qquad(17)$$

where ρ is the density of the material of the shell.

In the calculations an element of the non-moment shell similar to the one described in [4] with only three degrees of freedom per node was also used.

Fig. 6 shows the second eigenmode of a shell type cylinder with clamped edges. The constructed moire fringe patterns in the three directions of the coordinate axes are presented in Fig. 7, Fig. 8 and Fig. 9.

Isolines of displacements in those directions are constructed to validate the formation of isothethes (Fig. 10, Fig. 11 and Fig. 12).

Conclusions

Plotting of moire fringes from the results of finite element calculations is important because of the ability of direct comparisons with the experimental results of analysis. The smooth variation of the intensity of the lines on the surface of the structure according to the trigonometric law is proposed. The method is applied to the visualisation of the three dimensional vibrations of shell type structures by stroboscopic photographing of the structure in the state of equilibrium and in the state of extreme deflections.

The thickness of the lines on the surface of the three dimensional structure is not necessarily constant. So the

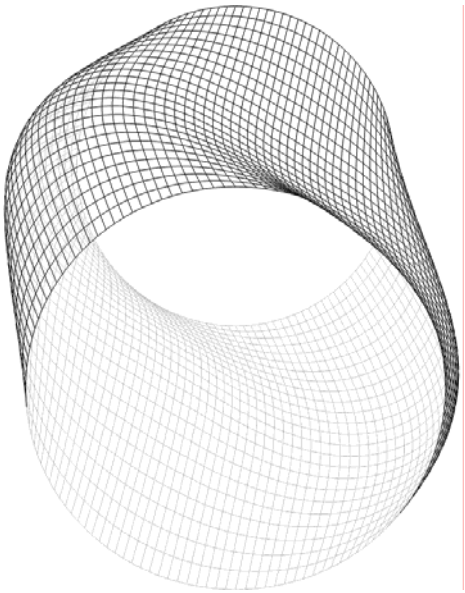

Fig. 6. **The second eigenmode of the cylindrical shell**

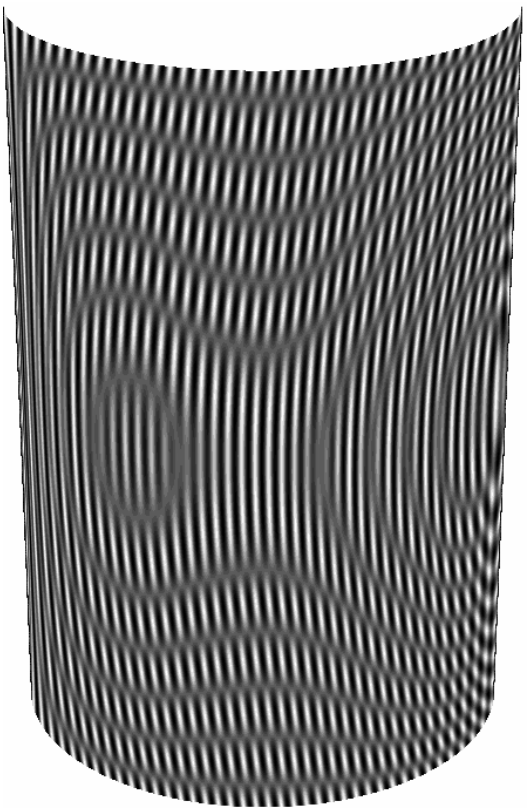

Fig. 7. **Moire fringes for the displacement in the direction of *x* axis**

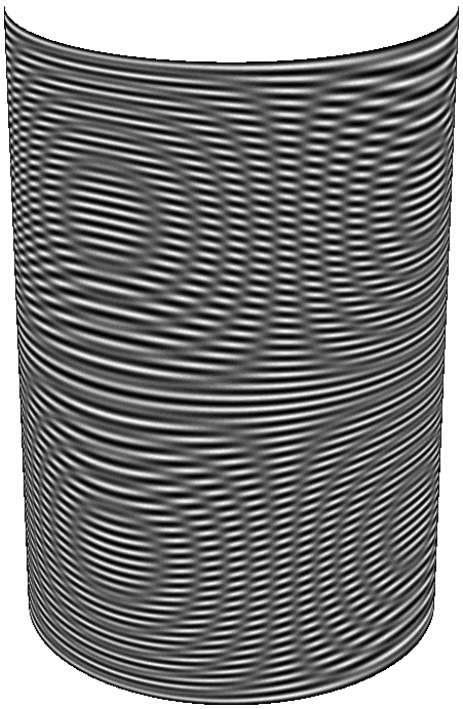

Fig. 8. **Moire fringes for the displacement in the direction of *y* axis**

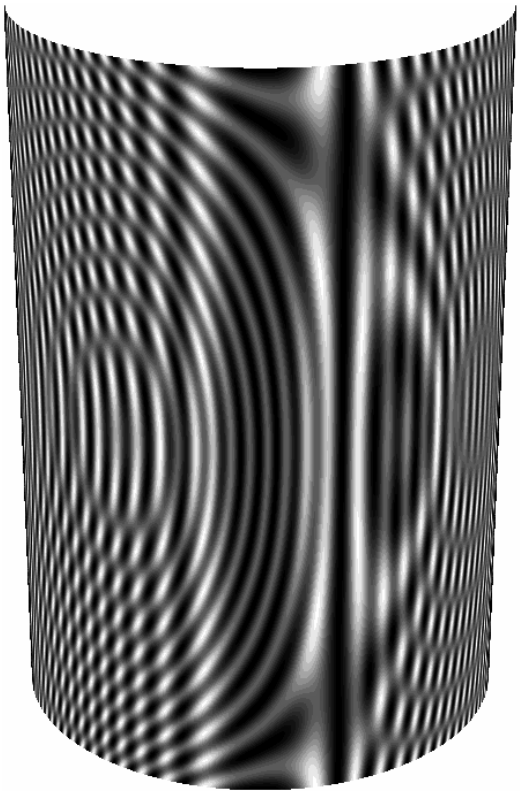

Fig. 9. **Moire fringes for the displacement in the direction of *z* axis**

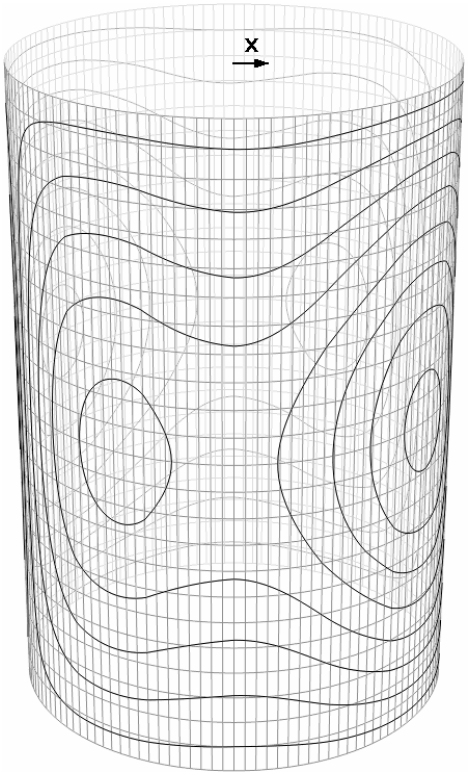

Fig. 10. **Izolines of the displacement in the direction of *x* axis**

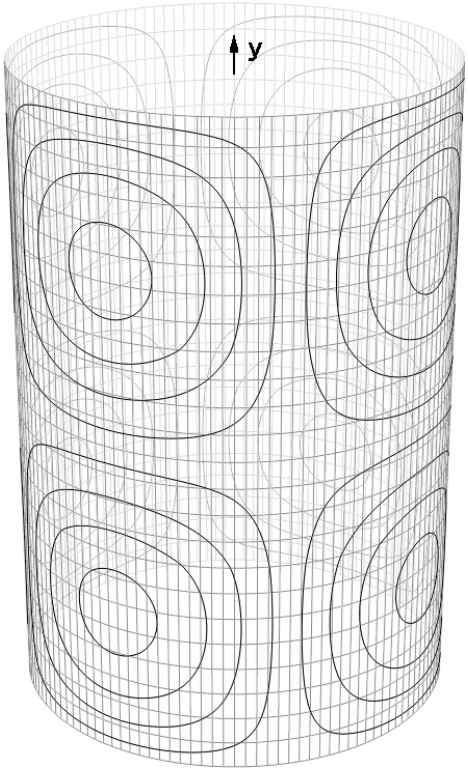

Fig. 11. .**Izolines for the displacement in the direction of *y* axis**

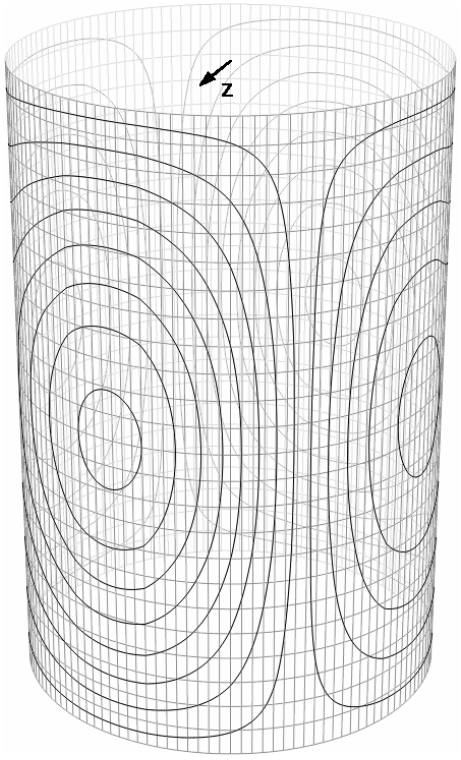

Fig. 12. **Izolines for the displacement in the direction of z axis**

application of the method to such problems is more difficult than to the two dimensional ones, but the results obtained numerically show interpretable moire patterns.

The procedure of numerical formation of moire fringes can be applied in the process of planning of experimental investigation enabling the selection of optimal spacing between the lines. Another useful application of the numerical method is the identification of the structural parameters when comparison between optical and simulated patterns can help to detect such physical values like the modulus of elasticity.

References:

1. **Timoshenko S. P., Goodier J. N.** Theory of elasticity. Moscow: Nauka. 1975.
2. **Soifer V. A.** Computer processing of images. Herald of the Russian Academy of Sciences. 2001. Vol. 71(2). P.119-129.
3. **Zienkiewicz O. C., Morgan K.** Finite elements and approximation. Moscow: Mir. 1986.
4. **Obrazcov I. F., Savieljiev L. M., Hazanov H. S.** The method of finite elements in the problems of building mechanics of flying devices. Moscow: Vysshaja shkola. 1985. P.392.
5. **Bathe K. J.** Finite element procedures in engineering analysis.New Jersey, Prentice-Hall, 1982.
6. **Ramesh K. and Pathak P. M.** Role of photoelasticity in evolving discretization schemes for FE analysis. J. Experimental Techniques, July/August 1999. P.36-38.

7. **Vest C.** Holographic interferometry. Moscow: Mir. 1982.
8. **Post D., Han B. T., Ifju P. G.** Moire methods for engineering and science. Moire interferometry and shadow Moire, Photo – mechanics topics in applied physics. 2000. Vol. 77. P.151-196.
9. **Han B., Post D., Ifju P.** Moire interferometry for engineering mechanics: current practices and future developments. Journal of strain analysis for engineering design. 2001. Vol. 36(1). P.101-117.

M. Ragulskis, L.Ragulskis

Moire juostų formavimas aukštuoju dažniu virpančioms kevalinėms struktūroms

Reziumė

Sujungiant skaičiavimo rezultatus su baigtinių elementų metodo dinaminės analizės rezultatais, sukurtos Moire interferencinės juostos kevalo tipo struktūroms. Naudojama kintamo pločio interferencinė gardelė, kuriai reikia atitinkamai modifikuoti skaitines procedūras.

Pateikta spaudai 2002 02 15

DOI: 10.5755/j01.u.42.1.8104